Elastic constants of Beryllium: a first-principles investigation

Andrea Dal Corso

International School for Advanced Studies (SISSA),

Via Bonomea 265, 34136 Trieste (Italy) and

DEMOCRITOS IOM-CNR Trieste

(Dated: January 13, 2016)

Abstract

We apply several recently introduced projector-augmented wave, ultrasoft, and norm-conserving pseudopotentials (PPs) to the calculation of the elastic constants of Beryllium and compare with previous theory and experiment. We discuss how the elastic constants depend on the Brillouin zone integration, on the PP type, and on the exchange and correlation functional. We find that although, in percentage, the elastic constants of Beryllium depend on the PPs more than the crystal parameters or the bulk moduli, the differences between the local density approximation (LDA) and the PBE generalized-gradient approximation are larger than the PPs differences. LDA overestimates experiment while PBE, which remains above experiment, gives a much better agreement than LDA. The PBEsol functional gives values slightly higher than PBE with differences comparable to the PPs uncertainty. We propose a simple formula to rationalize the internal relaxations in hcp crystals and show that Be relaxations are in reasonable agreement with this formula. The effects of internal relaxations on the values of C_{11} and C_{12} amount to a few percent of C_{11}, but up to 50 % of C_{12}.

PACS numbers: 62.20.D, 71.15.-m, 71.15.Mb, 81.05.Bx

I. INTRODUCTION

The structural, electronic, elastic, dynamical, and thermodynamic properties of solids are nowadays routinely calculated by density functional theory or similar methods.[1] High-throughput calculations can screen thousands or ten thousands of solids to search for a desired property.[2] Pseudopotentials (PPs) libraries that deal efficiently with all atoms of the periodic table have been built so that plane waves calculations and all-electron methods are converging on a similar accuracy.[3–6] However, many more efforts are needed before the tools of electronic structure theory can become black boxes usable by non specialists to engineer the properties of materials. Different functionals and different PPs require much more tests and the computation of physical quantities must become much more automatic. There are now sets of solids, whose number can reach a hundred or more, for which accurate all-electron data are available to make comparisons but usually only a few properties such as the crystal parameters, the bulk moduli, or the cohesive energies are investigated.[7–9] Comparisons on the phonon dispersions are more rare and not made in a systematic fashion.[10–12] Anharmonic properties and temperature dependent thermodynamic quantities are even less systematically investigated.[11] Likewise, elastic constants, especially those of anisotropic solids, are rarely used as benchmarks for the comparison of different numerical approaches.[13,14] Actually, it can happen that the theoretical values of these quantities reported by different authors have a large spread so that it is interesting to see how the recently developed PPs libraries behave in these critical cases.

The elastic properties of Beryllium are a paradigmatic example. Beryllium has been the focus of theoretical interest since the beginning of quantum mechanical electronic structure calculations.[15–17] With only four electrons per atom and two valence electrons, which in the atom fill the $2s$ shell, Beryllium appears as a simple metal, but the description of its properties has been a source of continuous debates and discussions. At standard conditions, it has the hexagonal close-packed structure with two atoms per cell and a c/a ratio of 1.568, smaller than the ideal 1.633, a fact that points to the existence of partially covalent bonds in addition to the metallic bond. The peculiar electronic structure gives Beryllium quite high elastic constants and a very small average Poisson ratio that together with the low density make it an interesting material from a practical point of view.

The elastic properties of Beryllium have been measured several times (See Ref. 18 and

references therein). While there is a certain agreement on the values of C_{11}, C_{33}, and C_{44}, the values of C_{12} and C_{13} have larger percentage errors. C_{11} is 2936 kbar in Ref. 18 at room temperature and has deviations up to about ± 140 kbar (± 5 %) in previous works, C_{33} is 3567 kbar in Ref. 18 and has deviations up to about ± 200 kbar (± 6 %), C_{44} is 1622 kbar in Ref. 18 and has deviations up to about ± 80 kbar (± 5 %), neglecting Ref. 19 that finds 1100 kbar and the value 1350 kbar quoted in Ref. 18. C_{12} is 268 kbar in Ref. 18 with deviations up to about -120 kbar (-45 %) (neglecting Ref. 19 that found a negative value), and C_{13} is 140 kbar with deviations up to about -90 kbar (-64 %) (neglecting Ref. 20 that found a negative value). Ab-initio elastic properties of Beryllium have been calculated many times [13,17,21–25] and the reported values have more spread than experiment. Some differences are due to the use of different exchange and correlation functionals, but even using the same functional the differences are somewhat larger than expected from the precision of the electronic structure methods.

In this paper we apply to this problem the recently developed projector-augmented wave (PAW) and ultrasoft (US) PPs libraries[3,4] focusing in particular on the PPs of `pslibrary`[26] but also comparing the GBRV US-PPs of Ref. 4, the norm-conserving (NC) PPs distributed with `pslibrary` and an older NC PP. We reconsider the numerical problem of evaluating the elastic constants of an hexagonal solid by finite differences and study the dependence of the calculated quantities on the Brillouin zone sampling. Moreover we compare three exchange and correlation functionals presenting results for the local density approximation (LDA),[27] the Perdew, Burke, and Ernzerhof (PBE)[28] generalized gradient approximation (GGA), and the PBEsol functional[29] that gives often structural properties of solids more accurate than PBE at the price of a worse description of atomization and cohesive energies. We present also a package under development, `thermo_pw`,[30] for the calculation of thermodynamic properties of solids and give some details on the part that calculates the elastic constants of hexagonal solids at zero temperature.

II. THEORY

There are several methods to calculate the elastic constants of an hexagonal solid. These are based either on the numerical differentiation of the stress or of the total energy[21,23,31] or on the analytic differentiation of the stress using the linear response theory.[32–35] The latter

approach, much more elegant theoretically and simpler to use, has been presented so far only for NC-PPs. In this paper we will focus on a finite differences approach, but since there are several equivalent expressions in the literature, as a reference, in this section we summarize the expressions implemented in `thermo_pw`. Theoretically, a given strain is imposed on a solid introducing a strain tensor ϵ_i ($i = 1, 6$ is a Voigt index) that changes the size and shape of the unit cell. Experimentally, to put the crystal in a strained state one applies a stress described by a tensor σ_i. Until the strains remain small, σ_i and ϵ_i are proportional:[36]

$$\sigma_i = \sum_{j=1}^{6} C_{ij}\epsilon_j. \tag{1}$$

The coefficients C_{ij} form a fourth-rank tensor and are called elastic constants (or elastic stiffness). In an hexagonal solid this tensor has the form:[37]

$$C = \begin{pmatrix} C_{11}, & C_{12}, & C_{13}, & 0, & 0, & 0 \\ C_{12}, & C_{11}, & C_{13}, & 0, & 0, & 0 \\ C_{13}, & C_{13}, & C_{33}, & 0, & 0, & 0 \\ 0, & 0, & 0, & C_{44}, & 0, & 0 \\ 0, & 0, & 0, & 0, & C_{44}, & 0 \\ 0, & 0, & 0, & 0, & 0, & C_{66} \end{pmatrix}, \tag{2}$$

with $C_{66} = (C_{11} - C_{12})/2$. C_{11}, C_{12}, and C_{13} can be obtained applying a strain ϵ_1 and calculating σ_1, σ_2, and σ_3, C_{33} by applying ϵ_3 and calculating σ_3, and C_{44} by applying ϵ_5 and calculating σ_5. This approach requires $N_\sigma = 3$ strains to obtain the five independent components of the elastic constants tensor. ϵ_3 changes the height c of the unit cell, and hence the c/a ratio, but does not change its hexagonal shape, ϵ_1 transforms the hexagonal lattice into a base-centered orthorhombic lattice, and ϵ_5 transforms it into a base-centered b-unique monoclinic lattice.

Alternatively the elastic constants can be calculated from the total energy of the strained solid. The total energy is a quadratic function of strain and, calling E_0 the energy of the equilibrium configuration at zero temperature and pressure, for a strain ϵ_1 it is:

$$E = E_0 + \frac{1}{2}C_{11}\epsilon_1^2. \tag{3}$$

For a strain ϵ_3 it is:

$$E = E_0 + \frac{1}{2}C_{33}\epsilon_3^2, \tag{4}$$

and for a strain ϵ_5 it is:

$$E = E_0 + \frac{1}{2} C_{44} \epsilon_5^2. \tag{5}$$

These three equations give C_{11}, C_{33}, and C_{44}. Applying a strain in which $\epsilon_1 = \epsilon_3 = \epsilon$, we have:

$$E = E_0 + \frac{1}{2}(C_{11} + C_{33} + 2C_{13})\epsilon^2, \tag{6}$$

that can be used to obtain C_{13} after computing C_{11} and C_{33}. Finally applying an isotropic strain $\epsilon_1 = \epsilon_2 = \epsilon_3 = \epsilon$, we have:

$$E = E_0 + \frac{1}{2}(2C_{11} + 2C_{12} + 4C_{13} + C_{33})\epsilon^2, \tag{7}$$

where the only unknown is C_{12}. Using these energy-strain relationships, we need $N_\sigma = 5$ strains to obtain the five independent components of the elastic constants tensor. The latter two strains are not substantially different from those described above. As ϵ_1, a strain with $\epsilon_1 = \epsilon_3 = \epsilon$ transforms the hexagonal lattice into a base-centered orthorhombic lattice but now also c is changed so that the c/a ratio remains constant. Similarly, as with ϵ_3, with the isotropic strain the lattice remains hexagonal and both a and c change, so that the c/a ratio remains constant.

A stress applied to a solid induces a strain that, for small stresses, is proportional to the stress:

$$\epsilon_i = \sum_{j=1}^{6} S_{ij} \sigma_j, \tag{8}$$

where the coefficients S_{ij} form a fourth-rank tensor and are called elastic compliances (or elastic moduli). In Voigt notation the 6×6 matrix S_{ij} is the inverse of the elastic constants matrix $S_{ij} = C_{ij}^{-1}$. The bulk modulus B can be computed by applying a uniform pressure $\sigma_1 = \sigma_2 = \sigma_3 = -p$ and measuring the volume change $\Delta V = V(\epsilon_1 + \epsilon_2 + \epsilon_3)$. We have:[38]

$$B = -V \frac{p}{\Delta V} = \frac{1}{S_{11} + S_{22} + S_{33} + 2S_{12} + 2S_{13} + 2S_{23}}. \tag{9}$$

We used this formula to calculate the bulk modulus from the elastic compliances obtained inverting the elastic constants matrix.

III. TECHNICAL DETAILS

Density functional theory calculations were carried out within the LDA,[27] PBE,[28] and PBEsol[29] exchange and correlation functionals using the `thermo_pw`[30] package, a FORTRAN

user interface that calls the routines of Quantum ESPRESSO[39] (QE) as the underlying engine. We applied the PPs of `pslibrary`[26] with core $1s$ electrons.[40] A few data have been obtained with PPs with $1s$ valence electrons,[40] and with the GBRV PPs of Ref. 4 version 1.4 (that have $1s$ electrons in valence). Moreover in order to compare our numerical approach with previous results, we have used the `Be.pz-n-vbc.UPF` PP available from the QE PPs web page. All PPs with core $1s$ electrons use the nonlinear core correction[41] for the exchange and correlation energy. The pseudo wavefunctions (charge density) have been expanded in plane waves with kinetic energy cut-offs of 35 Ry (300 Ry for PAW and US PPs, 140 Ry for NC PPs) for the PPs with $1s$ electrons in the core, 105 Ry (500 Ry) for the PPs with valence $1s$ electrons and 55 Ry (400 Ry) for the PPs of Ref. 4. These cut-offs give errors for the elastic constants of the same order or smaller than the other numerical uncertainties discussed in the next section. The presence of a Fermi surface has been dealt with by the smearing technique. We have compared three smearing approaches: Fermi-Dirac (FD), Methfessel-Paxton (MP),[42] and Marzari-Vanderbilt (MV).[43] The convergence of the calculated elastic constants with the **k**-points mesh and with the smearing parameter is described in the next section.

The formulas written in the previous Section have been implemented in the `thermo_pw` package.[30] Each of the N_σ strains has been applied to the unperturbed solid determined from the energy minimization. The equilibrium geometry has been re-optimized for each set of parameters by interpolating the energy calculated on a $N_e \times N_e$ grid of values of a and c/a with a second order polynomial and finding the minimum. We used $N_e = 5$ and varied a in steps of 0.01 a.u. form -0.02 a.u. to 0.02 a.u. and c/a in steps of 0.005 from -0.01 to 0.01, starting from a previous cell relaxation. For each of the N_σ strains, the stress-strain values obtained for $N = 4$ strains ranging from $\epsilon = -0.0075$ to $\epsilon = +0.0075$ in steps of 0.005 have been interpolated by a quadratic polynomial obtaining the elastic constant from the coefficient of the linear term. Instead $N = 6$ values of the energy-strain relationship from $\epsilon = -0.0125$ to $\epsilon = +0.0125$ in steps of 0.005 have been interpolated by a third-order polynomial obtaining the elastic constant from the coefficient of the quadratic term. For each strain, the ionic positions are strained uniformly (keeping them fixed in crystal coordinates). In general, when the atomic positions are strained uniformly, forces might appear on the atoms when they do not vanish for symmetry reasons. In this case, we minimize the energy until the forces are below 5×10^{-5} Ry/a.u., so the calculated elastic constants are already

corrected for internal relaxations and are directly comparable to experiment.

The `thermo_pw` code can make simultaneously and asynchronously many self-consistent calculations (or atomic relaxations) adding an additional level of parallelization to the standard methods of the QE routines. This additional level becomes useful when the number of processors exceeds the parallelization ability of the QE routines. In principle, the calculation of the elastic constants tensor can use a factor $N \times N_\sigma$ more processors than the QE routines doing in parallel all the self-consistent calculations (or atomic relaxations). The final result is obtained in the same elapsed time of a single relaxation for the strained geometry that requires more time.

IV. NUMERICAL ISSUES

We start this Section by discussing the convergence of the elastic constants with the smearing parameter (η) and the **k**-point sampling. We study three smearing functions FD, MP, and MV. For each smearing function, we fix the smearing parameter and calculate the elastic constants for several **k**-point grids. We consider three values of η and **k**-point meshes $N_k \times N_k \times N_{k_z}$ centered on the origin, where $(N_k, N_{k_z}) = (16, 10)$, $(20, 14)$, $(32, 24)$, $(40, 28)$, $(48, 32)$, $(64, 40)$, $(80, 54)$, $(96, 64)$, $(128, 86)$. In Fig. 1 we show C_{11}, C_{12}, C_{13}, C_{33}, and C_{44} as a function of N_k using the PAW PP of `pslibrary.1.0.0` with core $1s$ electrons. For MP and MV smearing we used $\eta = 0.04$ Ry, 0.02 Ry, 0.01 Ry, while for FD smearing $\eta = 0.02$ Ry, 0.01 Ry, 0.005 Ry. For clarity we have joined with a line the values of the elastic constants corresponding to the first two η (thin line for the first value and thick line for the second) while the third η is shown with points. For $\eta = 0.02$ Ry, the MP function, and $N_k = 128$ the values of the elastic constants are $C_{11} = 3352$ kbar, $C_{12} = 338$ kbar, $C_{13} = 117$ kbar, $C_{33} = 4096$ kbar, and $C_{44} = 1772$ kbar. Assuming that these values are converged, we indicate with two horizontal lines the range of values differing by $\pm 2\%$. C_{11}, C_{33}, and C_{44} are large, ± 2 % of these values correspond to ± 67 kbar, ± 82 kbar, and ± 35 kbar, respectively. C_{12} and C_{13} are instead quite small, ± 2 % correspond to ± 7 kbar and ± 2 kbar, respectively. Therefore it is relatively easy to calculate C_{11}, C_{33}, and C_{44}, with an error smaller than ± 2 % but it is very difficult to do the same for C_{12} and C_{13}.

Larger values of η require less **k**-points to converge, but the result is affected by the smearing error. The MP and the MV smearing functions have been especially tailored to

minimize the smearing error so that the energy has no quadratic dependence on η and converges to the $\eta = 0$ limit faster than using the FD function. This is actually the case in Fig. 1 for the elastic constants. Using $\eta = 0.02$ Ry and FD smearing the final values of C_{11}, C_{33}, C_{44}, and C_{12} have smearing errors close to the ± 2 % lines. The smearing error for C_{13}, of about 37 kbar, is in percentage larger. With $\eta = 0.01$ Ry and FD smearing the elastic constants are much closer to the converged results but still C_{13} is slightly outside the ± 2 % range. The other two functions, MP and MV, converge more rapidly with the smearing η. Both functions are within the ± 2 % limit for $\eta = 0.02$ Ry, and even $\eta = 0.04$ Ry gives values close to the converged ones with an accuracy similar to the FD smearing with $\eta = 0.01$ Ry. All three smearing functions give the same final values of the elastic constants within a few kbar, but a tight convergence threshold of less than 5 kbar for all the elastic constants requires $\eta = 0.02$ Ry for the MP function, $\eta = 0.01$ Ry for the MV function and $\eta = 0.005$ Ry for the FD function, the MP function having the fastest convergence with η. However, at fixed η the number of **k** points needed to converge within 5 kbar is different for the three functions. Actually, for the same η the FD smearing is the fastest to converge and with $\eta = 0.02$ Ry requires only $N_k = 20$, while the MP function requires $N_k = 80$ and the MV function requires $N_k = 64$. Therefore, depending on the target precision, different conclusions are reached on the most convenient function to use. An accuracy of 5 kbar on all elastic constants needs $\eta = 0.02$ Ry and $N_k = 80$ with MP smearing, $\eta = 0.01$ and $N_k = 96$ with MV smearing and $\eta = 0.005$ Ry and $N_k = 96$ with FD smearing. Accepting an error of 37 kbar on C_{13} and errors close to ± 2 % for the other elastic constants it is possible to use $\eta = 0.02$ Ry, FD smearing, and $N_k = 20$. A better accuracy on C_{13} and similar accuracy on the other elastic constants can be obtained with more effort using $\eta = 0.04$ Ry, MP or MV smearings and $N_k = 40$. Repeating the study of the **k**-points convergence with the `Be.pz-n-vbc.UPF` PP we found similar curves, so in Tab. I our calculated data have been obtained with MP smearing, $\eta = 0.02$ Ry, and $N_k = 80$ for all functionals and PPs without further testing.

The stress-strain or the energy-strain interpolation could also introduce some errors. In our calculations reported in Tab. I we used the stress-strain relationship. The use of $N = 4$ and of a quadratic interpolation introduces errors of the same order of magnitude as the **k**-point sampling. With $N = 6$, the same strain interval (0.005), and a third-order polynomial interpolation we obtained differences of 4 kbar, -1 kbar, 0 kbar, 0 kbar, -3 kbar, with

the LDA-PAW PP. Here and in the following discussion, we report the errors in the elastic constants as a set of fives numbers that refer to C_{11}, C_{12}, C_{13}, C_{33}, and C_{44} respectively. The energy-strain relationships, using LDA-PAW (LDA-US) PP, $N = 6$ and a strain interval of 0.005 differ from the stress-strain relationships by 22 (-5) kbar, -4 (-3) kbar, -1 (14) kbar, 7 (-16) kbar, and 0 (-3) kbar (using MP smearing, $\eta = 0.02$ Ry, $N_k = 80$). Larger strain intervals (0.02) reduce the differences between the elastic constants calculated from stress-strain or energy-strain, but with this larger strains higher order elastic constants effects become relevant and the stress-strain and energy-strain relationships must be interpolated at least with a third-order and a fourth-order polynomial, respectively. In this case, with the stress-strain relationships and $N = 6$ we found differences of the order of 1 (1) kbar, -1 (-1) kbar, 0 (1) kbar, -5 (5) kbar, 1 (-3) kbar with respect to the converged values written in Tab. I, and the differences between energy-strain and stress-strain calculation become 5 (6) kbar, -4 (-3) kbar, 9 (2) kbar, 5 (3) kbar, and -4 (0) kbar.

In the last panel of Fig. 1 we show the bulk modulus calculated from the elastic compliances (Eq. 9). This quantity converges more rapidly than the elastic constants. With all the smearings and **k**-point meshes discussed in this paper the bulk modulus is within the ± 2 % lines. Actually with the exception of the FD smearing with $\eta = 0.02$ Ry that differs by about 8 kbar from the converged value, all the other parameters give values in the range ± 5 kbar.

V. RESULTS AND DISCUSSION

We report in Tab. I all our calculated values of the elastic constants of Beryllium and compare them with previous calculations and with the experimental values of Ref. 18. We start by discussing the LDA case. The first six rows are our own calculations with the PAW and US PPs of `pslibrary.1.0.0` with core 1s electrons, with the NC PP distributed with `pslibrary.1.0.0`, with the PAW PP of the same library with 1s electrons in valence, with the US PP of the GBRV library[4] (that has 1s electrons in valence) and with the NC PP `Be.pz-n-vbc.UPF`. The seventh row contains the values found in Ref. 21 with a NC PP, energy-strain relationships slightly different from those described here, and the QE package. Other two theoretical calculations reported in Tab. I used the VASP code (Refs. 22,23), the one in Ref. 23 accounting for vibrational zero-point effects. We have compared also the

results of Ref. 17 that contains information on C_{33} and C_{13} obtained from the structural optimization.

There is a substantial agreement between our calculation made with the `Be.pz-n-vbc.UPF` PP and the results of Ref. 21 with differences of the same order of the numerical errors discussed above: -47 kbar (-2 %), 93 kbar (35 %), -26 kbar (-19 %), 71 kbar (2 %), and 17 kbar (1 %). The largest error is for C_{12} and it is compatible with the stronger dependence of C_{12} on the numerical details of the calculation and with the fact that this elastic constant depends on the internal strain (see next section). The two VASP calculations are more distant from these results and among themselves. For instance the difference between Ref. 21 and Ref. 22 is 258 kbar (9), -513 kbar (-191 %), 74 kbar (53 %), -585 kbar (-16 %), and -119 kbar (7 %). The differences between the two VASP calculations Ref. 22 and Ref. 23 are -115 kbar (-4 %), 305 kbar (114 %), -92 kbar (-66 %), 857 kbar (24 %), -58 kbar (-4 %), values that cannot be attributed only to the zero-point motion and point to the sensitivity of the elastic constants of Beryllium to all the details of the calculation. Finally the partial calculations in Ref. 17 for C_{33} and C_{13} are in agreement with Ref. 22.

The values obtained with the PPs of `pslibrary` are in agreement among themselves and with the results of the GBRV US PP of Ref. 4. For instance the difference between the PPs of the two libraries with valence $1s$ electrons are 9 kbar (0 %), -5 kbar (-2 %), -7 kbar (-5 %), 15 kbar (0 %), and 10 kbar (1 %), values that are within our numerical uncertainties. The PPs with core $1s$ electrons have slightly larger differences. For instance the difference between LDA-PAW values with and without the $1s$ electrons in the core are 24 kbar (1 %), 8 kbar (3 %), 5 kbar (4 %), 29 kbar (1 %), and 9 kbar (1 %). However there are quite marked differences between the values obtained with the PPs of the new libraries and the LDA values reported so far in the literature. The differences between our LDA-PAW result and Ref. 21 are 240 kbar (8 %), 146 kbar (54 %), -74 kbar (-53 %), 500 kbar (14 %), and 151 kbar (9 %). Refs. 22 and 17 are in agreement with our values as far as C_{33} and C_{13} are concerned, but the value $C_{12} = 708$ kbar found in Ref. 22 is about twice our value and C_{11} is about 500 kbar smaller than our value.

The values of the theoretical lattice parameters are instead in agreement and cluster about $a = 2.235 \pm 0.015$ Å and $c/a = 1.58 \pm 0.01$ and also the bulk moduli calculated with all methods are quite close, with our results and Ref. 22 close to 1300 kbar and Ref. 21 close

to 1200 kbar. Tab. I reports also the average Poisson ratio, calculated by using the Voigt-Reuss-Hill approximation.[44] The values of this parameter are quite stable with respect to the PPs and range from 0.052 to 0.057, similarly to the calculations available in the literature with the exception of Ref. 22 that with a C_{12} much larger than the other calculations gives an average Poisson ratio of 0.092.

Being higher than the previously reported LDA values that were already higher than experiment, the LDA elastic constants calculated with the the PPs of the recently developed libraries overestimate experiment by a large amount (with the exception of C_{13} that is smaller). The LDA-PAW errors are 413 kbar (14 %), 73 kbar (27 %), −23 kbar (−16 %), 528 kbar (15 %), 150 kbar (9 %) and similar values are found for the other PPs. A part of these errors is due to thermal effects, because the experimental data are at room temperature while our calculations are at $T = 0$ and neglect zero-point motion. Increasing temperature, the elastic constants decrease (except C_{13}). Experimentally the differences between low and room temperature have been estimated to be : 71 kbar (2 %), 9 kbar (3 %), −30 kbar (−21 %), 58 kbar (2 %), and 37 kbar (2 %).[45] These effects reduce the LDA errors, which however remain significant (with the exception of C_{13} that now would be 7 kbar (5 %) above experiment). These figures are in agreement with the general tendency of LDA to overestimate the bond strength.

We now pass to the discussion of the PBE case. The first four PBE rows of Tab. I are our calculations with the PAW and US PPs of `pslibrary.1.0.0`, with core 1s electrons, the NC PP distributed with `pslibrary.1.0.0` and the US PP of the GBRV library[4] (that has 1s electrons in valence). In the following rows we report previous calculations. Four calculations were made with VASP, but one of them[24] was at the experimental density. The other three (Refs. 13,22,46) were at the optimized geometry and can be directly compared with our calculation. Two VASP calculations[13,22] use the PW91 functional,[47] which should be equivalent to the PBE functional which is a simplification of it. Finally the last row refers to a calculation made with an all-electron LMTO code.[25]

Except for Ref. 46 that finds a somewhat larger value of a and smaller value for c/a, the PBE structural parameters are in remarkable agreement among themselves with $a = 2.263 \pm 0.004$ Å, and $c/a = 1.576 \pm 0.004$. There is also a general agreement on the bulk moduli, all calculations giving values 1220 ± 15 kbar except the last two (Refs. 24 and 25) that give 1133 kbar and 1125 kbar. However, the first calculation is at the experimental

density and the other uses the HL functional[48] for the LDA part. PBE decreases the elastic constants with respect to LDA (except C_{13} that is similar to LDA). For instance with the PAW PP of `pslibrary.1.0.0` with core 1s electrons the PBE-LDA differences are -214 kbar (-7 %), -44 kbar (-16 %), 3 kbar (2 %), -285 kbar (-8 %), and -96 kbar (-6 %). Here again our PAW, US, and NC PPs calculations are in agreement among themselves. Moreover the values found with the new libraries are in agreement with those of Ref. 13. For instance PBE-PAW differs of 13 kbar (0 %), 51 kbar (19 %), 11 kbar (8 %), 31 kbar (1 %), and 22 kbar (1 %) from this reference. The differences with Ref. 46 are instead slightly larger -87 kbar (-3 %), 84 kbar (31 %), 40 kbar (28 %), 28 kbar (1 %), and 57 kbar (4 %). Also Refs. 24,25 are in reasonable agreement with our results with the exception of C_{33} which is 520 kbar and 215 kbar smaller than our values, respectively. Ref. 22 instead finds C_{13}, C_{33}, and C_{44} in agreement with our calculation, but C_{11} is 539 kbar smaller than our PBE-PAW value and C_{12} is 393 kbar higher. The PBE elastic constants remain above experiment (except C_{13}) and have errors smaller than LDA. The differences between PBE-PAW and experiment are 199 kbar (7 %), 29 kbar (11 %), -20 kbar (-14 %), 243 kbar (7 %), and 54 kbar (3 %). Including thermal effects estimated experimentally the errors become: 128 kbar (5 %), 20 kbar (8 %), 10 kbar (7 %), 185 kbar (5 %), and 17 kbar (1 %). The average Poisson ratios become slightly lower than LDA and cluster about the experimental value 0.050, with the exception of Ref. 22 that as in the LDA case has a value, 0.093, larger than all the other calculations. Note also that Ref. 24,25 find values 0.036 and 0.030 slightly lower than our values.

The PBEsol[29] functional has been shown to give improved crystal parameters of solids and for many metals it can give quite accurate phonon dispersions,[12] at the same computational cost of PBE. For phonon frequencies it is particularly useful when LDA overestimates experiment and PBE underestimates it because it gives results that are intermediate among the two functionals. However, as shown in Ref. 12, the improvements of the structural properties and of the phonon frequencies are not always correlated with an improvement of the bulk moduli. The usefulness of PBEsol for elastic constants has been analyzed in a recent paper for cubic insulators and semiconductors finding that PBEsol performs better than both LDA and PBE.[14] In Tab. I we report our calculations with the PAW and US PPs of `pslibrary.1.0.0` and with the NC PP distributed with this library, together with the results given by the GBRV US PPs of Ref. 4. From the data reported in Table I we see

that the elastic constants calculated with the PBEsol functional are slightly higher than the PBE ones (with the exception of C_{13} which is smaller), but quite close to them, so that the differences between PAW, US, and NC PPs are of the same order of the differences between PBEsol and PBE results. With the PAW PP we find that these differences are 48 kbar (2 %), 6 kbar (2 %), −21 kbar (−15 %), 70 kbar (2 %), and 20 kbar (1 %). With the GBRV PPs these differences are 25 kbar (1 %), 1 kbar (0 %), −20 kbar (−14 %), 38 kbar (1 %), and 11 kbar (1 %). We conclude that also for this particular problem, PBEsol is intermediate between LDA and PBE and, although much closer to PBE and almost indistinguishable from it, it goes in the LDA direction and therefore slightly worsen the agreement with experiment with respect to PBE.

VI. INTERNAL STRAIN

The hexagonal close-packed structure has two atoms per cell and forces might appear on the atoms when a uniform strain is applied to all atomic coordinates,[49] so that the atoms relax in a different configuration. In these cases, "frozen-ions" elastic constants calculated by uniformly straining the atoms without further relaxation might differ from the total or "relaxed-ions" elastic constants. Two of the three strains considered in this paper, ϵ_1 and ϵ_5, allow an internal relaxation, while ϵ_3 does not. However, as discussed in Ref. 49, only ϵ_1 gives relaxations proportional to the strain. ϵ_5 gives relaxations that, depending quadratically on the strain, do not change appreciably C_{44}. Therefore only the frozen-ions values of C_{11} and C_{12} differ from the total values. C_{13}, which can be calculated from both ϵ_1 and ϵ_3, does not change when calculated with frozen or relaxed ions.

In this section we present some results about the calculated internal relaxations for ϵ_1. In Fig. 2 we show the geometry of this strain. Three atoms A, B, and C belong to one hexagonal layer and one atom, X, to the layer at height $c/2$ from this. The orthorhombic cell and a few repeated atoms are also shown. a is the side of the hexagonal cell. In the unstrained configuration, A, B, and C form an equilateral triangle and X is at the same distance from these three atoms. A strain ϵ_1 (of amplitude ϵ), illustrated in Fig. 2b, changes the side the orthorhombic cell in the x direction to $a(1+\epsilon)$ and does not change any length in the y and z directions. The atoms A, B, and C now form an isosceles triangle. A uniform strain of the coordinates of X according to ϵ_1 does not change its y coordinate so

the distance of X from A and B is the same but the distance from C is different. The reduced symmetry now allows X to move in the y direction (together with all atoms in the same sublattice). Writing the coordinates of X as $X = (\frac{1+\epsilon}{2}, y, \frac{c}{2a})$ in units of a, we have $AX^2 = BX^2 = \left(\frac{1+\epsilon}{2}\right)^2 + y^2 + \left(\frac{c}{2a}\right)^2$, while $CX^2 = \left(y - \frac{\sqrt{3}}{2}\right)^2 + \left(\frac{c}{2a}\right)^2$. Requiring that $AX^2 = BX^2 = CX^2$ we find that y is:

$$y = \frac{1}{\sqrt{3}}\left(\frac{1}{2} - \frac{1}{2}\epsilon - \frac{1}{4}\epsilon^2\right). \tag{10}$$

In general y will have a value that depends on the bonds present in the solid and must be calculated by energy minimization. We can take Eq. 10 and the uniform strain as two reference values and compare them with the calculated equilibrium positions.

In Fig. 3 we compare Eq. 10 with the y coordinate calculated ab-initio from the energy minimization using the LDA and PBE PAW PP of `pslibrary.1.0.0` and the `Be.pz-n-vbc.UPF` LDA-NC PP. The horizontal line $y = \frac{\sqrt{3}}{6}$ shows the value of y obtained after a uniform strain, while the points show the final y coordinate (in units of a). For the small strains ± 0.0075 used in our elastic constants calculation Eq. 10 is on top of the calculated displacements according to the LDA-PAW PP and remain correct also for larger strains up to ± 0.05. The LDA-NC PP predicts instead slightly smaller relaxations. The slope of the y-strain line is -0.23 to be compared with the value $-\frac{1}{2\sqrt{3}} = -0.289$ predicted by Eq. 10. The PBE-PAW PP predicts also slightly smaller relaxations than Eq. 10 and the slope is -0.26.

In Tab. II we report the values of the frozen-ions elastic constants and compare them with the total ones. The effect on C_{11} and C_{12} is quite large. Theoretically[50] it has been shown that within an embedded-atom potential model $\Delta C_{11} = -\Delta C_{12}$ and this relationship is well verified in our calculation. The frozen-ions values of C_{11} differ by $\Delta C_{11} = 170$ kbar (+5 % for C_{11}, -50 % for C_{12}) with the LDA-PAW PP, $\Delta C_{11} = 106$ kbar (+3 % for C_{11}, -37 % for C_{12}) with the LDA-NC PP and $\Delta C_{11} = 134$ kbar (4 % for C_{11}, -45 % for C_{12}) with the PBE-PAW PP. The other elastic constants are instead unaffected by the ionic relaxations for the reasons discussed before. One can also see that in the orthorhombic geometry a change of the y position of the atom X does not change the σ_3 component of the stress, so that C_{13} calculated using ϵ_1 is not affected by the ionic relaxations. Very small changes, smaller than 1 kbar, are found between frozen-ions and total values of C_{44}. In agreement with Ref. 49, we find that the relaxations after a strain ϵ_5 are quadratic in the strain as the

change of the distances between nearest neighbor atoms in the hexagonal planes. Therefore only the elastic constants of order higher than the second are affected by these relaxations.

Our calculated values reported in Tab. I have been obtained relaxing the atoms, but it is not clear if the frozen or relaxed ions values have been reported in the literature. Part of the discrepancies found in previous section for C_{11} and C_{12} could be due to a different treatment of the ionic relaxations.

VII. CONCLUSIONS

We have used `pslibrary.1.0.0`[26] and the GBRV library[4] to calculate the elastic constants of Beryllium. We have found that the calculated values are rather sensitive to all the numerical parameters. The convergence with respect to the **k**-point sampling has been studied in detail and, although the final values depend on this sampling, different **k**-point convergences cannot explain the large spread of the values found in the literature. In the LDA case, we do not agree completely with any previous reference and find that with the new PPs libraries the Beryllium elastic constants are higher than those reported so far. In the PBE case we agree with Ref. 13.

LDA overestimates experiment and PBE corrects a large part of the LDA error. It remains higher than experiment and it is much closer. With the new PPs libraries, the differences between elastic constants calculated with PAW, US, and NC PPs are, in percentage, larger than the differences found for the crystal parameters or the bulk moduli but smaller than the LDA-PBE differences. They are comparable to the PBEsol-PBE differences.

We have also analyzed the ionic relaxations for the strain ϵ_1, the only strain that in the hexagonal close-packed structure induces displacements proportional to the strain and can influence the second-order elastic constants. The relaxations in Beryllium are well explained by the tendency of the atoms to stay at the same distance from all the three nearest-neighbor atoms on the planes above and below. Internal relaxations change C_{11} and C_{12} and in percentage have a small effect (of a few percent) on C_{11} but a large effect (up to 50 %) on C_{12}.

Acknowledgments

Computational facilities have been provided by SISSA through its Linux Cluster and ITCS, by DEMOCRITOS through its Linux Cluster, and by CINECA thought the SISSA-CINECA 2015 agreement. This work has been supported by MIUR through PRIN 2010-11 (Registration number 20105ZZTSE_005).

---

[1] S. Baroni, S. de Gironcoli, A. Dal Corso, and P. Giannozzi, Rev. Mod. Phys. **73**, 515 (2001).

[2] C. Toher, J.J. Plata, O. Levy, M. de Jong, M. Asta, M.B. Nardelli, and S. Curtarolo, Phys. Rev. B **90**, 174107 (2014).

[3] A. Dal Corso, Comput. Material Science **95**, 337 (2014).

[4] K.F. Garrity, J.W. Bennett, K.M. Rabe, and D. Vanderbilt, Comp. Mater. Sci. **81**, 446 (2013).

[5] F. Jollet, M. Torrent, and N. Holzwarth, Comput. Phys. Commun. **185**, 1246 (2014).

[6] K. Lejaeghere, et al., in preparation.

[7] P. Haas, F. Tran, and P. Blaha, Phys. Rev. B **79**, 085104 (2009). P. Haas, F. Tran, and P. Blaha, Phys. Rev. B **79**, 209902(E) (2009).

[8] A. Dal Corso, Phys. Rev. B **86**, 085135 (2012).

[9] K. Lejaeghere, V. Van Speybroeck, G. Van Oost, and S. Cottenier, Crit. Rev. Solid State **39**, 1 (2014).

[10] F. Favot and A. Dal Corso, Phys. Rev. B. **60**, 11427 (1999).

[11] B. Grabowski, T. Hickel, and J. Neugebauer, Phys. Rev. B **76**, 024309 (2007).

[12] A. Dal Corso, J. Phys.: Condens. Matter **25**, 145401 (2013).

[13] S.L. Shang, A. Saengdeejing, Z.G. Mei, D.E. Kim, H. Zhang, S. Ganeshan, Y. Wang, and Z.K. Liu, Comp. Mater. Sci. **48**, 813 (2010).

[14] M. Råssander and M.A. Moram, arXiv:1505.02379.

[15] M.Y. Chou, P.K. Lam, and M.L. Cohen, Phys. Rev. B **28**, 4179 (1983).

[16] P. Blaha and K. Schwarz, J. Phys. F: Met. Phys. **17**, 899 (1987).

[17] N.A.W. Holzwarth and Y. Zeng, Phys. Rev. B **51**, 13653 (1995).

[18] A. Migliori, H. Ledbetter, D.J. Thoma, and T.W. Darling, J. Appl. Phys. **95**, 2436 (2004) and references therein. See in particular Table I.

[19] L. Gold, Phys. Rev. **77**, 390 (1950).

[20] D.J. Silversmith and B.L. Averbach, Phys. Rev. B **1**, 567 (1970).

[21] F. Luo, L.-C. Cai, X.-R. Chen, F.-Q. Jing, and D. Alfè, J. Appl. Physics **111**, 053503 (2012).

[22] L.G. Hector, Jr. and J.F. Herbst, W. Wolf, P. Saxe, and G. Kresse, Phys. Rev. B **76**, 014121 (2007).

[23] T. Shao, B. Wen, R. Melnik, S. Yao, Y. Kawazoe, Y. Tian, J. Appl. Physics **111**, 083525 (2012).

[24] G. Robert and A. Sollier, J. Phys. IV **134**, 257 (2006).

[25] G.V. Sin'ko and N.A. Smirnov, Phys. Rev. B **71**, 214108 (2005).

[26] See `http://www.qe-forge.org/gf/project/pslibrary/`.

[27] J.P. Perdew and A. Zunger, Phys. Rev. B **23**, 5048 (1981).

[28] J.P. Perdew, K. Burke, and M. Ernzerhof, Phys. Rev. Lett. **77**, 3865 (1996).

[29] J.P. Perdew, A. Ruzsinszky, G.I. Csonka, O.A. Vydrov, G.E. Scuseria, L.A. Constantin, X. Zhou, and K. Burke Phys. Rev. Lett. **100**, 136406 (2008).

[30] `Thermo_pw` is a set of `FORTRAN` drivers of the Quantum ESPRESSO routines that helps to speed up the most common tasks. The elastic constants reported in this paper have been calculated with the `scf_elastic_constant` and `mur_lc_elastic_constant` options. See `http://www.qe-forge.org/gf/project/thermo_pw/`.

[31] G. Steinle-Neumann, L. Stixrude, R.E. Cohen, Phys. Rev. B **60**, 791 (1999).

[32] S. Baroni, P. Giannozzi and A. Testa, Phys. Rev. Lett. **59**, 2662 (1987).

[33] D.R. Hamann, X. Wu, K.M. Rabe, and D. Vanderbilt, Phys. Rev. B **71**, 035117 (2005).

[34] D.R. Hamann, K.M. Rabe, and D. Vanderbilt, Phys. Rev. B **72**, 033102 (2005).

[35] X. Wu, D. Vanderbilt, and D.R. Hamann, Phys. Rev. B **72**, 035105 (2005).

[36] The stress tensor is calculated by the QE routines, using the stress theorem (O.H. Nielsen and R.M. Martin, Phys. Rev. B **32**, 3780 (1985)). The stress printed by the QE routines is the stress exerted by the solid in a given strained state and has opposite sign with respect to the stress written in Eq. 1.

[37] J.F. Nye, *Physical properties of crystals*, Oxford University press, Oxford (1957). In the present paper positive stresses are defined as in this reference.

[38] D.C. Wallace, Thermodynamics of crystals, Dover publications, New York (1972).

[39] P. Giannozzi, et al., J. Phys.: Condens. Matter **21**, 395502 (2009). See `http://www.quantum-espresso.org`.

[40] We used the datasets `Be.pz-n-kjpaw_psl.1.0.0.UPF`, `Be.pz-n-rrkjus_psl.1.0.0.UPF`, `Be.pz-n-nc.UPF`, `Be.pbe-n-kjpaw_psl.1.0.0.UPF`, `Be.pbe-n-rrkjus_psl.1.0.0.UPF`, `Be.pbe-n-nc.UPF`, `Be.pbesol-n-kjpaw_psl.1.0.0.UPF`, `Be.pbesol-n-rrkjus_psl.1.0.0.UPF`, `Be.pbesol-n-nc.UPF`, and `Be.pz-sl-kjpaw_psl.1.0.0.UPF`.

[41] S.G. Louie, S. Froyen, and M.L. Cohen, Phys. Rev. B **26**, 1738 (1982).

[42] M. Methfessel and A. T. Paxton, Phys. Rev. B **40**, 3616 (1989).

[43] N. Marzari, D. Vanderbilt, A. De Vita, and M.C. Payne, Phys. Rev. Lett. **82**, 3296 (1999).

[44] R.E. Newnham, *Properties of Materials: Anisotropy, Symmetry, Structure*, Oxford University Press (2005). The average Poisson ratio has been calculated for a polycrystalline solid using the Equations at page 115 of this reference, correcting the factor 5 in the Reuss expression of the Young's modulus to 3 (See for instance J.M.J. den Toonder, J.A.W. van Dommelen and F.P.T. Baaijens, Modelling Simul. Mater. Sci. Eng. **7**, 909 (1999).)

[45] J.F. Smith and C.L. Arbogast, Jour. of Appl. Phys. **31**, 99 (1960).

[46] M. de Jong, W. Chen, T. Angsten, A. Jain, R. Notestine, A. Gamst, M. Sluiter, C. K. Ande, S. van der Zwaag, J. J. Plata, C. Toher, S. Curtarolo, G. Ceder, K. A. Persson, and M. Asta Scientific Data **2** 150009 (2015).

[47] J.P. Perdew, J.A. Chevary, S.H. Vosko, K.A. Jackson, M.R. Pederson, D.J. Singh, and C. Fiolhais, Phys. Rev. B **46**, 6671 (1992).

[48] L. Hedin and B.I. Lundqvist, J. Phys. C **4**, 2064 (1971).

[49] R.A. Johnson, Modelling Simul. Mater. Sci. Eng. **1**, 717 (1993).

[50] H.J.P. van Midden and A.G.B.M. Sasse, Phys. Rev. B **46**, 6020 (1992).

[51] K.J.H. Mackay and N.A. Hill, Jour. Nucl. Mat. **8**, 263 (1963). Data have been taken at temperature $T = 293.6$ K.

TABLE I: Elastic constants of Be calculated in the present work (using the data sets of `pslibrary` if not specified otherwise) compared with previous calculations and experimental results. The elastic constants and the bulk moduli (B) are in kbar. ν is the average Poisson ratio. Data in [e] include zero-point motion effects, all the others do not.

	a (Å)	c/a	C_{11}	C_{12}	C_{13}	C_{33}	C_{44}	B	ν
LDA-PAW	2.224	1.579	3349	341	117	4095	1772	1322	0.054
LDA-US	2.234	1.578	3306	346	132	4033	1743	1313	0.057
LDA-NC	2.234	1.578	3276	332	151	3977	1733	1305	0.058
LDA-PAW ($1s$)	2.226	1.579	3325	333	112	4066	1763	1310	0.053
LDA-US[a] ($1s$)	2.228	1.579	3316	338	119	4051	1753	1310	0.054
LDA-NC[b]	2.246	1.574	3062	288	165	3666	1638	1220	0.057
LDA-NC[c]	2.248	1.57	3109	195	191	3595	1621	1216	0.052[o]
LDA-PAW[d]	2.23	1.583	2851	708	117	4180	1740	1302	0.092[o]
LDA-PAW[e]	2.242	1.586	2966	403	209	3323	1798	1210[o]	0.057[o]
LDA[f]	2.23	1.574			100	4200		1400	
PBE-PAW	2.261	1.576	3135	297	120	3810	1676	1234	0.051
PBE-US	2.262	1.575	3117	302	122	3790	1669	1230	0.052
PBE-NC	2.259	1.575	3101	275	125	3740	1669	1216	0.049
PBE-US[g] ($1s$)	2.266	1.576	3105	306	127	3776	1656	1229	0.054
PW91-PAW[d]	2.26	1.580	2596	690	107	3916	1664	1207	0.093[o]
PW91-PAW[h]	2.263	1.579	3122	246	109	3779	1654	1211	0.046[o]
PW91-PAW[i]	2.287*	1.57	3059	188	104	3290	1593	1133[o]	0.036[o]
PW91**-FP-LMTO[j]	2.266	1.573	3008	141	71	3595	1602	1125[o]	0.030[o]
PBE-PAW[k]	2.280	1.547	3222	213	80	3782	1619	1215[o]	0.043[o]
PBEsol-PAW	2.253	1.577	3183	303	99	3880	1696	1245	0.049
PBEsol-US	2.260	1.577	3157	310	113	3840	1676	1243	0.052
PBEsol-NC	2.255	1.577	3152	292	121	3825	1683	1239	0.051
PBEsol-US[l] ($1s$)	2.263	1.577	3130	307	107	3814	1667	1230	0.051
Expt.[m]	2.285[n]	1.568[n]	2936	268	140	3567	1622	1168	0.050

[a] This work using `be_lda_v1.4.uspp.F.UPF`. See Ref. 4. [b] This work using `Be.pz-n-vbc.UPF`.
[c] Ref. 21, [d] Ref. 22, [e] Ref. 23, [f] Ref. 17. [g] This work using `be_pbe_v1.4.uspp.F.UPF`. See Ref. 4.
[h] Ref. 13, [i] Ref. 24, [j] Ref. 25. [k] Ref. 46.
[l] This work using `be_pbesol_v1.4.uspp.F.UPF`. See Ref. 4. [m] Ref. 18, [n] Ref. 51.
[o] Calculated from the elastic constants.
* Experimental value. ** the LDA part made with the functional of Ref. 48.

TABLE II: Effect of atomic relaxations on the elastic constants of Be. FI indicates a frozen-ions calculation in which the atomic positions are uniformly strained and kept fixed. The FI values are compared with the total relaxed-ions elastic constants. Two different PPs are compared in the LDA case (see text) and the LDA and PBE functionals are compared with the PAW PP.

	a (Å)	c/a	C_{11}	C_{12}	C_{13}	C_{33}	C_{44}	ΔC_{11}
LDA-PAW-FI	2.224	1.579	3519	170	117	4095	1772	170
LDA-PAW	2.224	1.579	3349	340	117	4095	1771	
LDA-NC-FI[a]	2.246	1.574	3168	183	165	3666	1639	106
LDA-NC[a]	2.246	1.574	3062	289	165	3666	1638	
PBE-PAW-FI	2.261	1.576	3269	162	120	3810	1676	134
PBE-PAW	2.261	1.576	3135	297	120	3810	1676	

[a] This work using `Be.pz-n-vbc.UPF`.

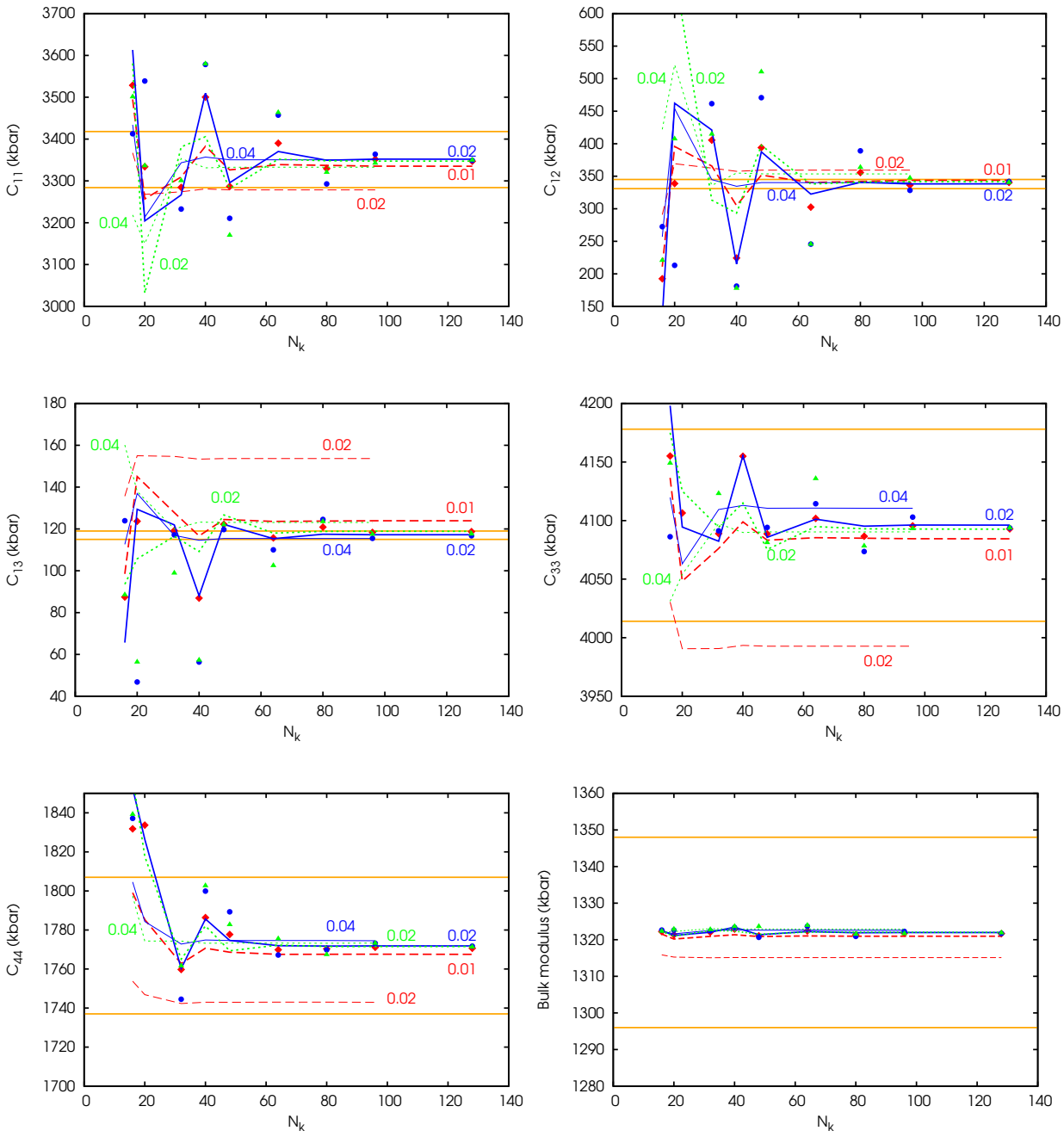

FIG. 1: (Color online) Elastic constants convergence with the number of **k**-points. The different lines types indicate different smearing functions: FD (red dashed lines), MP (blue lines) and MV (green dotted lines). The two linewidths indicate two values of the smearing parameters indicated (in Ry) and with the same color close to each line. A third value of the smearing is shown only with symbols. Red diamonds refer to a smearing of $\eta = 0.005$ Ry for FD, blue circles and green triangles to $\eta = 0.01$ Ry for MP and MV functions respectively. The horizontal lines indicate a range of ± 2 % with respect to the converged values. On the last panel we show the bulk modulus B_0 for comparison.

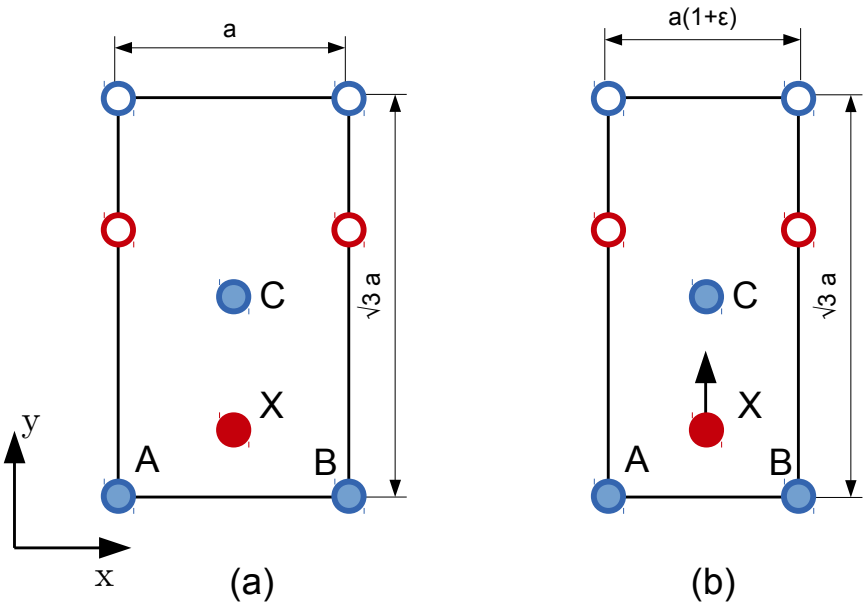

FIG. 2: (Color online) Schematic illustration of the ϵ_1 strain. (a) The hexagonal lattice is shown as an orthorhombic lattice projected in the xy plane. The blue atoms A, B, and C are in the same plane while the red atoms are in a plane at height $c/2$ from it. (b) A strain ϵ_1 changes one side of the orthorhombic cell. Straining uniformly the position of X brings the atom at the same distance from A and B, but not from C. The strain does not change the y coordinate of X, but the atom can relax along y because its y coordinate is not symmetry constrained.

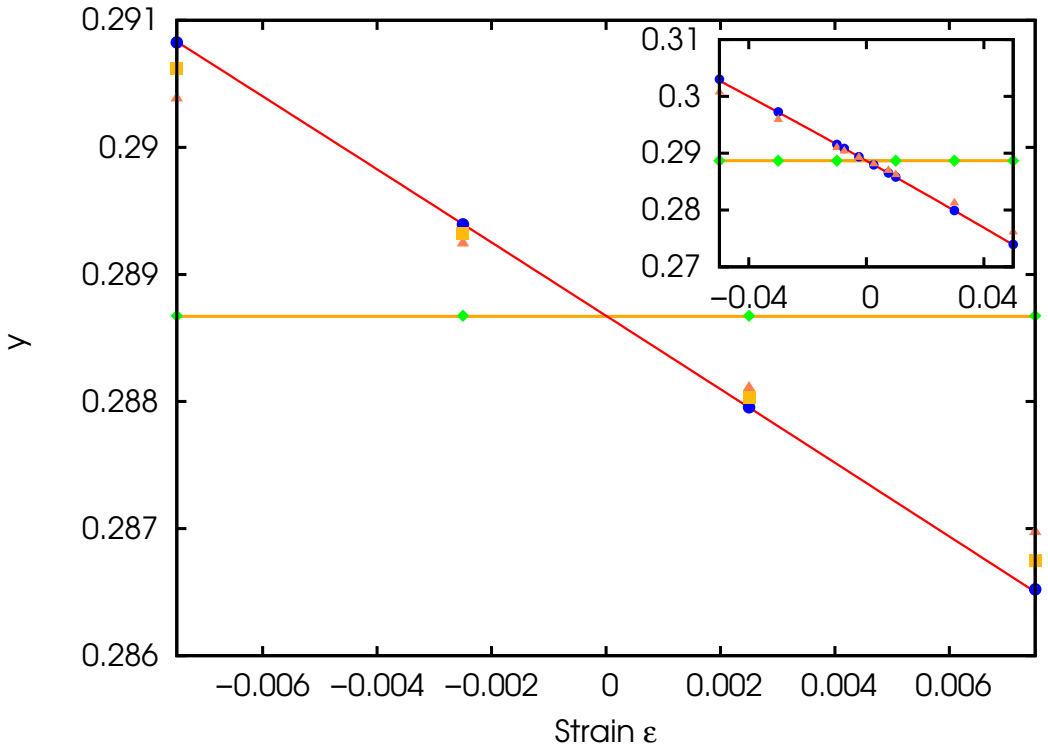

FIG. 3: (Color online) y coordinate of the atom X for different values of the amplitude of the strain ϵ_1 applied to the crystal. The red line is Eq. 10 while the symbols are the calculated values (circles for the LDA-PAW PP, triangles for the NC PP, and squares for the PBE-PAW PP). The horizontal line at $\sqrt{3}/6$ corresponds to a uniform strain applied to the coordinates of the X atom. The diamonds are the starting points of the relaxation. In the inset, the same figure for a larger range of strains without the squares.